

Scintillation modeling for GPS–Wide Area Augmentation System receivers

Christopher Hegarty, M. Bakry El-Arini, Taehwan Kim, and Swen Ericson
Center for Advanced Aviation System Development, The MITRE Corporation, McLean, Virginia

Abstract. A scintillation signal model and a Global Positioning System (GPS)–Wide Area Augmentation System (WAAS) receiver model are developed. The scintillation signal model is based on a Nakagami-m distribution for intensity and a Gaussian distribution with zero mean for phase. The GPS–WAAS receiver model includes Link 1 (L1) GPS and WAAS carrier- and C/A-code-tracking loops, as well as semicodeless Link 2 (L2) carrier and Y-code tracking capabilities. The results show that noncoherent delay locked loops (DLLs) typically used for code tracking are very robust to both amplitude and phase scintillation. Carrier-phase-tracking loops are much more susceptible to scintillation, and the signal-to-noise threshold for reliable carrier tracking is very dependent on the scintillation strength. Fortunately, it appears that the worst case scintillation encountered at midlatitudes, including the United States, does not significantly impact L1 carrier-tracking performance. Semicodeless tracking of the L2 carrier is shown to be very fragile. Even weak scintillation can cause loss of L2 carrier lock for low-elevation satellites.

1. Introduction

Scintillation causes radio frequency (RF) signal amplitude fading and phase variations as satellite signals pass through the ionosphere [Klobuchar, 1996; Aarons and Basu, 1994]. This effect could cause a receiver to “lose lock” on the ranging signals broadcast by Wide Area Augmentation System (WAAS) [Loh *et al.*, 1995] geostationary or GPS satellites, potentially causing a short service outage for one or more aircraft [Pullen *et al.*, 1998]. Scintillation occurs most frequently during the peak of the solar cycle. Scintillation may be severe in equatorial regions (geomagnetic equator $\pm 15^\circ$) after sunset and, to a somewhat lesser extent, the polar and auroral regions. Scintillation typically has minimum impact in midlatitude regions, e.g., the conterminous United States (CONUS).

The aviation community is interested in the answers to the following questions regarding

scintillation: (1) For what percentage of time will GPS and WAAS receivers lose lock for one satellite, two satellites, etc., in each of the regions noted above? (2) What is the impact of scintillation on the availability of WAAS (and GPS in general) in the United States and worldwide? This paper will try to answer the first question. The second question will be answered in a future paper because it requires the incorporation of a scintillation model into a WAAS service volume model.

To better understand the impact of scintillation on WAAS (and GPS) operations, the MITRE Center for Advanced Aviation System Development has developed a scintillation signal model and also a GPS/WAAS receiver model. The scintillation signal model is based on a Nakagami-m distribution for intensity and a Gaussian distribution with zero mean for phase. The GPS/WAAS receiver model includes L1 GPS and WAAS carrier- and C/A-code-tracking loops, as well as semicodeless L2 carrier- and Y-code-tracking capabilities.

The four scintillation levels shown in Table 1 are considered in this paper. These levels were generated using the Wideband Ionospheric

Copyright 2001 by the American Geophysical Union.

Paper number 1999RS002425.
0048-6604/01/1999RS002425\$11.00

Table 1. Scintillation Cases Considered

Case	S_4 at L1	$\sigma_{\delta\phi}$ at L1, rad
Strong	0.9	0.6
Moderate	0.6	0.3
Weak	0.4	0.2
Very weak	0.1	0.05

Scintillation Model (WBMOD) [Secan, 1996] and are felt to be representative of the range of scintillation intensity that may be encountered in the equatorial region during various phases of the 11 year solar cycle and various local times. The scintillation parameter S_4 is the ratio of the standard deviation of the intensity of the received signal to its mean. The other parameter listed in the table, $\sigma_{\delta\phi}$ is the standard deviation of the scintillation phase variations. It should be noted that WBMOD defines the variance of scintillation phase variations as being the integral of the phase perturbation power spectral density (PSD) from a user-selectable parameter to infinity. The $\sigma_{\delta\phi}$ values in Table 1 were produced by WBMOD using a lower limit of 0.1 Hz.

Figure 1 shows the modeled change in S_4 for two GPS satellites between 2000 and 2330 local solar time (LST), for Honolulu, Hawaii. The top of the figure shows the ionospheric pierce point (IPP) paths of the signals' intersections with the ionosphere at an altitude of 350 km. During this time the elevation angles of PRN 21 and PRN 25 vary from approximately 8° to 70° and 37° to 6° , respectively. Note that the value of S_4 increases after local sunset, as expected [Klobuchar, 1996; Aarons and Basu, 1994], and decays slowly afterward. The value of S_4 for PRN 25 increases toward the end of its path because the satellite is setting and scintillation tends to be stronger at lower elevation angles. The values of S_4 are high since the IPP paths go through the equatorial region. This example was generated with WBMOD using the following input variables: Frequency equals 1575.42 MHz, sunspot number (SSN) equals 150 (approximately the peak of solar cycle), Kp index equals 4 (average geomagnetic activity), day of the year is 50, and local time of the receiver is ~ 2030 – 2310 LST (after sunset).

2. Scintillation Signal Model

The received signal at the GPS-WAAS receiver is assumed to be

$$E = Ae^{j\phi} = E_0 \delta E = (A_0 \delta A) e^{j(\phi_0 + \delta\phi)}, \quad (1)$$

where $E_0 = A_0 e^{j\phi_0}$ is the nominal received signal (without scintillation) with nominal amplitude A_0 and nominal phase ϕ_0 and $\delta E = \delta A e^{j\delta\phi}$ is the scintillation signal with amplitude δA and phase $\delta\phi$.

The scintillation signal is modeled as a Nakagami-m distribution for intensity and zero-mean Gaussian distribution for the phase. Correlation between intensity and phase is also considered. The Nakagami-m distribution is given by Nakagami [1960]

$$f(\delta A) = \frac{2m^m \delta A^{2m-1}}{\Gamma(m)\Omega^m} e^{-m\delta A^2/\Omega} \quad \delta A \geq 0, \quad (2)$$

$$f(\delta I) = \frac{m^m \delta I^{m-1}}{\Gamma(m)\Omega^m} e^{-m\delta I/\Omega} \quad \delta I = (\delta A)^2 \geq 0,$$

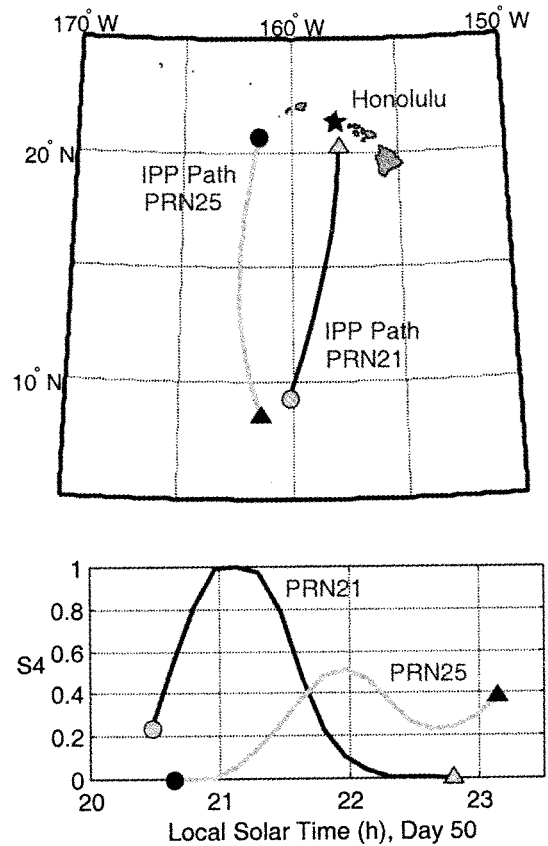


Figure 1. IPP arcs of two GPS satellites (PRN 21 and PRN 25) seen south of a GPS receiver at Honolulu, Hawaii. The scintillation parameter S_4 is also shown.

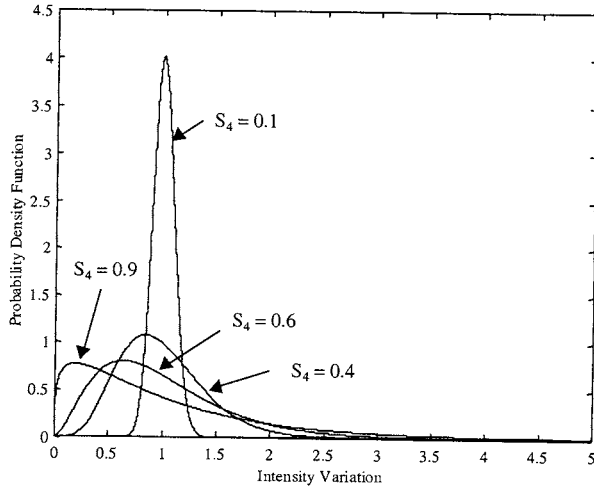


Figure 2. Intensity variation probability density functions.

where $\Omega = E(\delta A^2) = E(\delta I)$ is the average power of the signal, $\delta I = \delta A^2$ is the intensity of the scintillation signal, and m is given by

$$m = \frac{[E(\delta A^2)]^2}{E[\delta A^2 - E(\delta A^2)]^2} = \frac{[E(\delta I)]^2}{E[\delta I - E(\delta I)]^2} \quad (3)$$

$$= \frac{\Omega^2}{E(\delta I - \Omega)^2} = \frac{1}{S_4^2} \geq \frac{1}{2}$$

The intensity is characterized by the S_4 scintillation parameter

$$S_4 = \frac{\sigma_{\delta I}}{E(\delta I)} = \frac{\sqrt{E[\delta I - E(\delta I)]^2}}{E(\delta I)} \quad (4)$$

$$= \frac{\sqrt{E(\delta I - \Omega)^2}}{\Omega} \leq \sqrt{2}$$

and the phase is characterized by its standard deviation $\sigma_{\delta\phi}$. The probability density functions of intensity variations (equation (2)) corresponding to the S_4 values listed in Table 1 are plotted in Figure 2. Note that for the case $S_4 = 0.1$ it is very unlikely that signal intensity will drop below one half its nominal value (3 dB fade). When S_4 reaches values above 0.6, deep fades occur with increasing frequency.

2.1. Generation of the Scintillation Signal

The intensity and phase of the scintillation signal

are generated by a bivariate gamma random variable. The gamma marginal density functions considered are given by [Schmeiser and Lal, 1982]

$$f_i(x_i) = \frac{(x_i/\beta_i)^{(\alpha_i-1)} e^{-x_i/\beta_i}}{\beta_i \Gamma(\alpha_i)} \quad (5)$$

$$x_i \geq 0, \alpha_i \geq 0, \beta_i > 0, i = 1, 2,$$

and the correlation coefficient ρ is defined as follows:

$$\rho = \frac{E(x_1 x_2) - E(x_1)E(x_2)}{\sqrt{V(x_1)V(x_2)}} \quad (6)$$

$$= \frac{E\left(\frac{x_1}{\beta_1} \frac{x_2}{\beta_2}\right) - \sqrt{\alpha_1 \alpha_2}}{\sqrt{\alpha_1 \alpha_2}}$$

where $V(\)$ is the variance of its argument.

We assumed that x_i in (5) represents the intensity of the scintillation signal with the following relationships between gamma and Nakagami-m distributions [Pullen et al., 1998]:

$$\alpha_1 = m = \frac{1}{S_4^2}, \beta_1 = \frac{1}{m} = S_4^2, \quad (7)$$

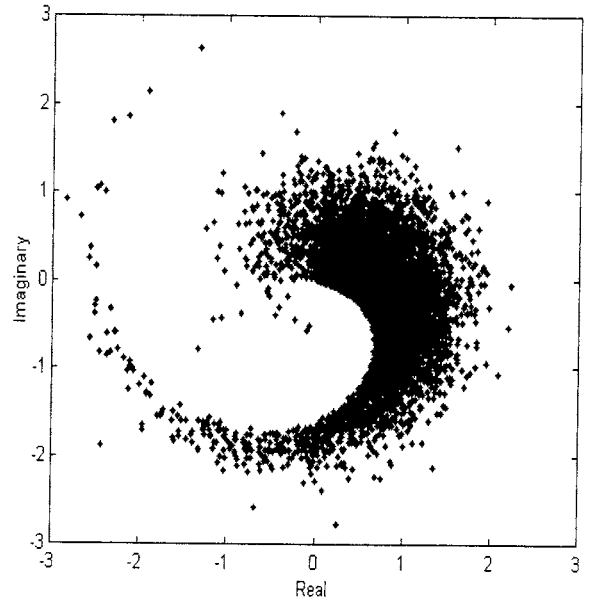


Figure 3. Scatterplot of scintillation signal in the complex plane ($S_4 = 0.9, \sigma_{\delta\phi} = 0.6$).

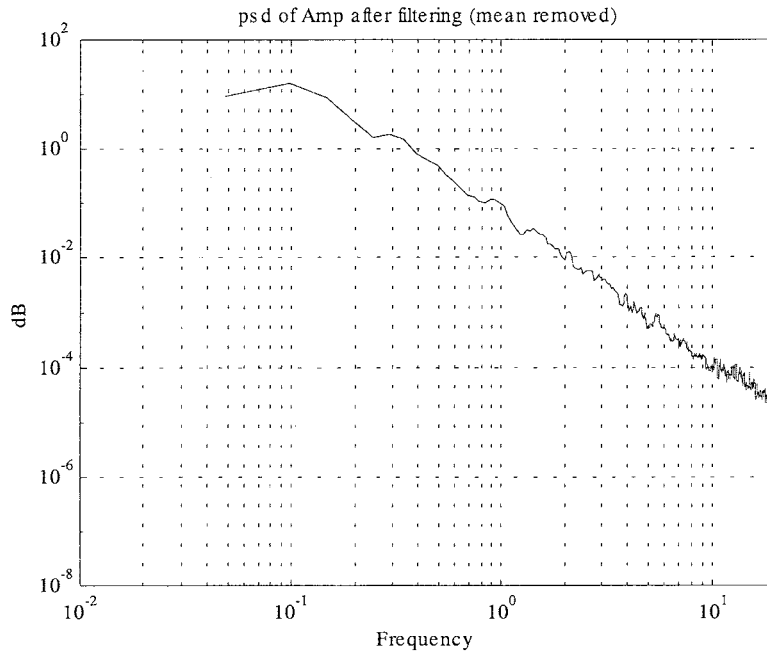


Figure 4. Amplitude PSD (mean removed), $S_4 = 0.6$.

and we also assumed that x_2 represents the phase with zero-mean Gaussian distribution. This can be done by assuming very large α_2 with $\beta_2 = 1$. After generating the joint intensity and phase distribution using the bivariate gamma random vector generator described below, the marginal Gaussian phase distribution is scalable to $N(0, \sigma_{\delta\phi})$ without affecting the correlation coefficient ρ between the intensity and phase components.

The trivariate reduction method [Devroye, 1986, p. 588] is used to generate bivariate gamma random vectors as follows: (1) Generate a gamma $(\alpha_1 - \rho\sqrt{\alpha_1\alpha_2})$ random variate G_1 , (2) Generate a gamma $(\alpha_2 - \rho\sqrt{\alpha_1\alpha_2})$ random variate G_2 , (3) Generate a gamma $(\rho\sqrt{\alpha_1\alpha_2})$ random variate G_3 , and (4) Return $X_1 = G_1 + G_2$, and $X_2 = G_2 - G_3$ (the minus sign in X_2 is used to generate negative correlation).

The range of the correlation coefficient is given by

$$-\frac{\min\{\alpha_1, \alpha_2\}}{\sqrt{\alpha_1\alpha_2}} \leq \rho \leq 0. \quad (8)$$

The generation of G_1 , G_2 , and G_3 from a single-variate gamma distribution is given also by Devroye [1986]. When $\alpha < 1$, the gamma distribution becomes exponential, and it can be generated using the transform method (inverse CDF) described by Devroye [1986, p. 405]. When $\alpha < 1$, the Johnk's gamma generator [Devroye, 1986, pp. 416–418] is used. When $\alpha > 1$, Best's rejection algorithm is used [Devroye, 1986, pp. 407–410].

Figure 3 shows the scatterplot of the scintillation signal, prior to spectral shaping, in the complex plane generated from the bivariate gamma distribution with correlation coefficient between intensity and phase at -0.6 , $S_4 = 0.9$, $\sigma_{\delta\phi} = 0.6$. Because of the strong correlation and large S_4 , the focus component E_f appears to be more dominant than the scatter component E_s of the signal $\delta E = E_s E_f$ [Fremouw et al., 1980].

Scintillation signal at L2 frequency is created independently by the trivariate reduction method. The phases of L1 and L2 are later correlated with the desired correlation coefficient (typically 0.9). S_4 and $\sigma_{\delta\phi}$ for L2 are determined using the following equations [Van Dierendonck et al., 1996]:

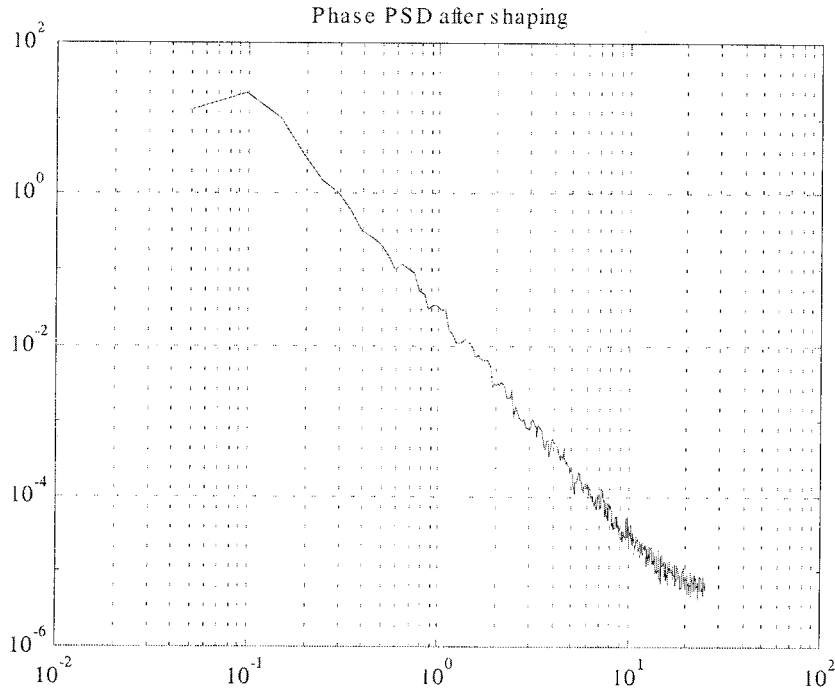


Figure 5. Phase PSD, $\sigma_{\delta\phi} = 0.3$ rad.

$$S_4(L2) = S_4(L1) \left(\frac{f_{L1}}{f_{L2}} \right)^{1.5} = 1.454 S_4(L1), \tag{9}$$

$$\sigma_{\delta\phi}(L2) = \sigma_{\delta\phi}(L1) \left(\frac{f_{L1}}{f_{L2}} \right) = 1.283 \sigma_{\delta\phi}(L1).$$

2.2. Spectral Shaping

To create realistic power spectral densities (PSD) for intensity variations [see, e.g., *Basu et al.*, 1987], two methods were used. For strong scintillation ($S_4 > 0.8$) a cascade of two second-order Butterworth filters (one low-pass and one high-pass) was used while for medium-to-weak scintillation ($S_4 \leq 0.8$) a technique from *Kasdin* [1995] (described later in this section) was used. In the first method, the cutoff frequencies of the low-pass and high-pass filters were 0.7 Hz and 0.1 Hz, respectively. (Note that the low order of the high- and low-pass filters results in a nonzero PSD both above and below the cutoff frequencies.) Figure 4 shows an example of the simulated intensity PSD after removing the mean value of 1. For the strong scintillation case of $S_4 = 0.9$ a high-frequency roll-off slope parameter of -5.5 was used [*Basu et al.*, 1987]. For the medium and weak S_4 cases, slopes of -3.0 to -2.5 were used, respectively.

The PSD of phase scintillation is known to follow the form $P_\phi(f) = T f^{-p}$, where f is frequency (hertz), T is a strength parameter (rad^2/Hz) corresponding to the power at 1 Hz, and p is a unitless slope that is typically $2.0-3.0$ [*Basu et al.*, 1987]. This ubiquitous autospectral density form, known as power law noise, may be accurately simulated by passing white noise through a digital filter with transfer response [*Kasdin*, 1995]:

$$H(z) = \frac{1}{(1 - z^{-1})^{p/2}} \quad z > 1. \tag{10}$$

As derived in *Kasdin* [1995], the power series expansion of this transfer function can be used to design an equivalent recursive infinite impulse response (IIR) autoregressive (AR) filter described by

$$x_n = -a_1 x_{n-1} - a_2 x_{n-2} - a_3 x_{n-3} - \dots + w_n, \tag{11}$$

$$a_0 = 1, \tag{12}$$

$$a_k = \left(k - 1 - \frac{p}{2} \right) \frac{a_{k-1}}{k}.$$

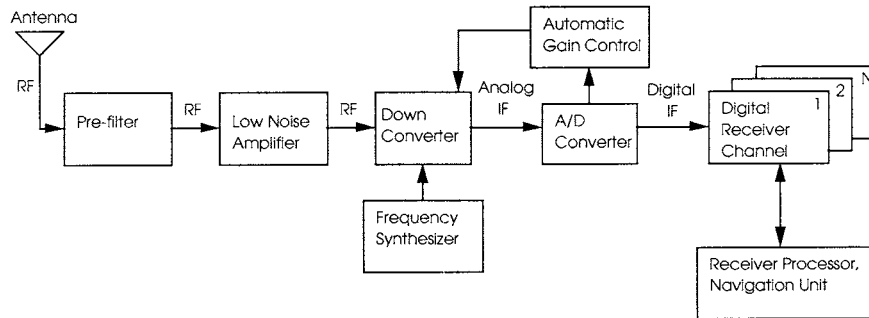


Figure 6. GPS receiver overview.

Although this filter was found to run slowly when implemented, it was chosen over an alternative frequency domain finite impulse response (FIR) filter implementation described by *Kasdin* [1995]. The latter implementation imposes a larger memory burden and limits data lengths to powers of 2 because of its reliance on the fast Fourier transform (FFT).

The resulting phase PSD is shown in Figure 5, where the slope value $p = 2.5$ was used with $\sigma_{\delta\phi} = 0.3$ rad. Note that a high-pass Butterworth filter with a cutoff frequency of 0.1 Hz is applied to facilitate vertically biasing the simulated phase scintillation PSD to match WBMOD outputs. Although phase scintillation does not exhibit any inherent low-frequency roll-off, low-frequency phase variations are of no significance with regard to the performance of GPS WAAS receiver tracking loops and thus may be ignored [*Pullen et al.*, 1998].

The spectral shaping resulted in a reduction of the cross correlation coefficient between intensity variations and phase variations from -0.6 to the lower range of values between -0.1 and 0.1 . This effect is understandable given the different desired spectral characteristics. Methods of achieving larger target values for the output cross-correlation are being investigated.

3. GPS-WAAS Receiver Modeling

A block diagram of a typical GPS C/A code receiver is shown in Figure 6 [*Ward*, 1995]. The RF signal is received by an L-band antenna. This signal is filtered and then amplified by a low-noise amplifier (LNA). Next, the signal is down-converted to a convenient intermediate frequency (IF) and converted from analog to digital (A/D). The digital signal is

then passed to a bank of N channels (see Figure 7 of *Ward* [1995]) that form complex sums of the correlation between the input signal and C/A code replicas. One channel is needed for each satellite to be tracked. The complex correlation sums are used by a processing unit to track the code and carrier of the received signals so that pseudoranges to each satellite can be estimated. The correlation sums are also used by the processor to demodulate the data modulating the satellite signals.

In this paper, we model L1 GPS-WAAS C/A code processing and semicodeless GPS L1 and L2 Y code processing using a baseband model [*Van Dierendonck et al.*, 1992; *Van Dierendonck*, 1996] that starts with the complex correlation sums produced by the generic receiver channel shown in Figure 7. For C/A code processing the integration periods $T_C = 20$ ms for GPS and $T_W = 2$ ms for WAAS are used. For semicodeless Y code processing the received signals on L1 and L2 are correlated with the P code over an integration period $T_Y = 1.96$ μ s (the deduced period of the underlying encryption code [*Hatch et al.*, 1992]).

For L1 C/A code tracking, a dot product discriminator [*Van Dierendonck et al.*, 1992; *Van Dierendonck*, 1996] is used in a first-order, carrier-aided noncoherent delay locked loop (DLL). The code-tracking (pseudorange) jitter variance of this DLL implementation, σ_{τ}^2 , in code chips (one GPS WAAS chip equals 293 m) squared may be expressed as [*Van Dierendonck et al.*, 1992; *Van Dierendonck*, 1996]

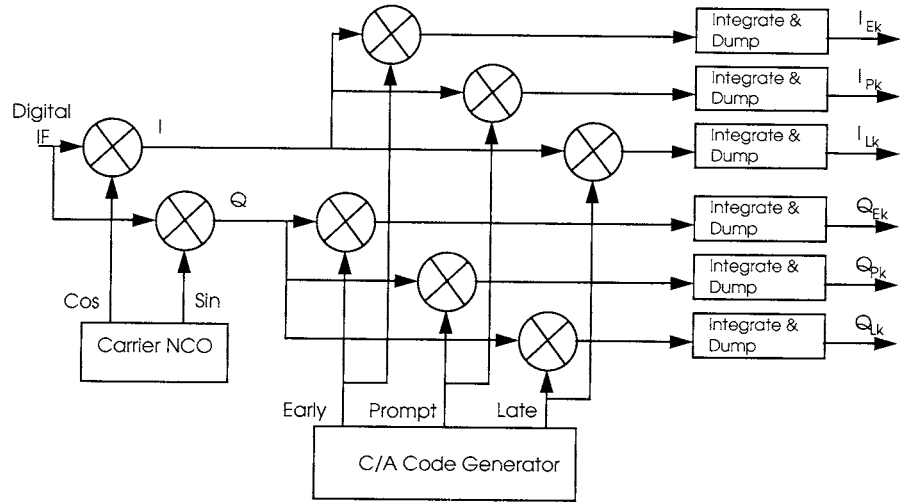


Figure 7. Receiver channel.

$$\sigma_{\tau}^2 = \frac{B_L d}{2S/N_0} \left[1 + \frac{1}{S/N_0 T} \right], \quad (13)$$

where B_L is the one-sided noise bandwidth of the code loop filter (set to 1/10 Hz in our simulations), d is the correlator chip spacing (one chip was simulated), S/N_0 is the input equivalent C/A code signal-to-noise power density, and T is the predetection integration time (20 ms for GPS, 2 ms for WAAS).

Carrier tracking is performed using the discriminator

$$d\phi_k = \arctan \left(\frac{Q_{Pk}}{I_{Pk}} \right). \quad (14)$$

A third-order loop using the design detailed by *Stephens and Thomas* [1995] is employed. The carrier-tracking jitter variance of the tracking loop σ_{ϕ}^2 , in radians squared, is approximately (neglecting oscillator effects) [*Van Dierendonck*, 1996]

$$\sigma_{\phi, \text{noise}}^2 = \frac{B_{\phi}}{S/N_0} \left[1 + \frac{1}{2S/N_0 T} \right], \quad (15)$$

where B_{ϕ} is the one-sided carrier loop bandwidth (typically 10–20 Hz) and T is the predetection integration time (20 ms for GPS and 2 ms for WAAS).

The semicodeless processing technique that was modeled [*Hegarty*, 1994] uses the prompt Q samples of a L1 P code correlator as soft (unquantized) estimates of the underlying encryption code bits to wipe off the encryption code from L2 P code correlator I and Q samples. After this wipe-off process the L2 P code I and Q samples are accumulated for 20 ms and used to feed tracking loops similar to those described above for the C/A code processing. The L2 Y-code-tracking jitter variance using this implementation is [*Hegarty*, 1994]

$$\sigma_{\tau}^2 = \frac{B_L}{2(S/N_0)_{L2P}} \left[1 + \frac{1}{2(S/N_0)_{L1P} T_Y} \right]. \quad (16)$$

The L2 carrier-tracking jitter variance is [*Hegarty*, 1994; *Woo*, 2000]

$$\sigma_{\phi}^2 = \frac{B_{\phi}}{(S/N_0)_{L2P}} \left[1 + \frac{1}{2(S/N_0)_{L1P} T_Y} \right]. \quad (17)$$

Note that incomplete knowledge of the Y code results in dramatic degradations in tracking accuracies [*Hegarty*, 1994; *Woo*, 2000; *Van Dierendonck*, 1994] (the second term in the square brackets is large because of T_Y being small). This degradation is typically partially compensated using L1 carrier aiding of the L2 loops, which allows the use of much lower loop bandwidths. The modeled receiver uses

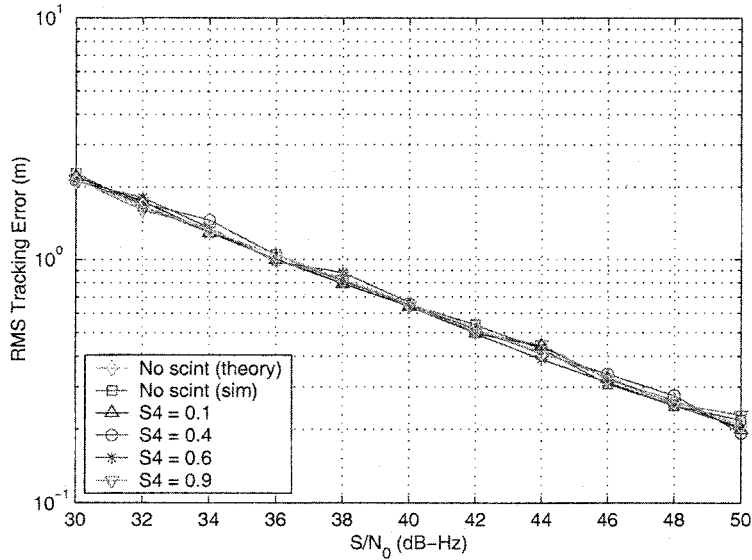


Figure 8. L1 C/A-code-tracking results.

L1 carrier aiding of all loops (L1 C/A code tracking and L2 carrier phase and Y code tracking).

4. Simulation Results

The results of simultaneously applying phase and amplitude scintillation, using our signal model, to the GPS L1 C/A code DLL model are shown in Figure 8. The figure plots the root-mean-square (RMS) code-tracking error (in meters) versus L1 C/A code signal-to-noise density ratio S/N_0 . Each point on the plot was determined using 45,000 simulation samples (15

min of simulated data at 50 Hz). Note that for all scintillation cases considered (S_4 ranging from 0 to 0.9), the modeled 1/10 Hz noncoherent DLL is very robust and did not display any degradation.

Results for the GPS L1 carrier tracking loop are shown in Figure 9. This figure shows the RMS carrier phase tracking jitter (in degrees) observed in the simulations, root-sum-squared with a typical value of oscillator-induced jitter (5.7° RMS [Hegarty, 1997]). An important carrier loop performance measure for many GPS applications is the mean time between cycle slips (called the mean time to lose

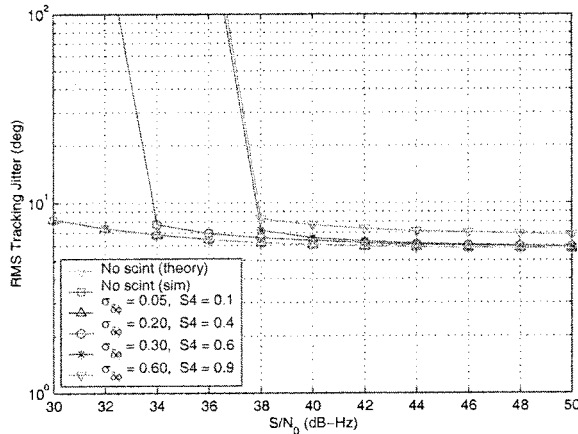


Figure 9. GPS L1 carrier-tracking results.

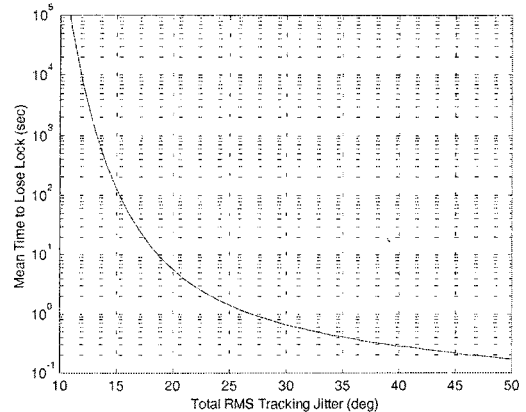


Figure 10. Mean time to lose lock vs. total RMS tracking jitter.

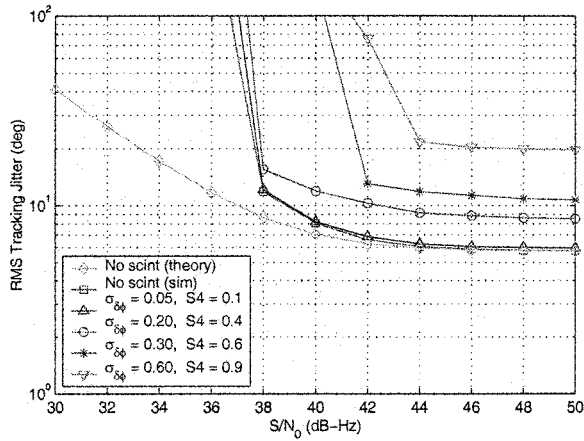


Figure 11. Semicodeless GPS L2 carrier-tracking results.

lock). The mean time between cycle slips \bar{T} for a first-order Costas loop is given by the following equation for the unstressed loop case [Holmes, 1990]:

$$\bar{T} = \frac{\pi^2}{8\sigma_{\delta\phi}^2 B_\phi} I_0^2\left(\frac{1}{4\sigma_{\delta\phi}^2}\right), \quad (18)$$

where B_ϕ is the loop bandwidth (10 Hz), and $I_0(\cdot)$ is the zeroth-order modified Bessel function of the first kind. Figure 10 shows the relationship between \bar{T} and $\sigma_{\delta\phi}$ for a first-order loop. Higher-order loops, used for dynamic platforms, typically exhibit much shorter (2–3 orders of magnitude) values of \bar{T} versus $\sigma_{\delta\phi}$ [Stephens and Thomas, 1995]. Depending on the loop order and the specific application, scintillation that causes $\sigma_{\delta\phi}$ to exceed 10° – 12° may cause unacceptably frequent cycle slips. For aviation applications, $\sigma_{\delta\phi}$ should be less than or equal to approximately 10° .

Loop performance is not noticeably degraded when weak and moderate scintillation ($\sigma_{\delta\phi} \leq 0.3$ rad) is present as shown in Figure 9. However, for the moderate and strong scintillation cases ($\sigma_{\delta\phi} \geq 0.6$ rad) the signal-to-noise ratio required to maintain continuous carrier tracking is significantly increased. For example, at $S/N_0 \leq 38$ dB Hz, the RMS tracking

jitter is abruptly increased because of cycle slips for the strong scintillation case.

Figure 11 shows the results for the semicodeless GPS L2 carrier tracking loop. Even with L1 carrier aiding and a narrow loop bandwidth (1/4 Hz), the loop is operating close to the break-lock threshold over a range of typical S/N_0 (L1 C/A code S/N_0 is the independent variable; L1 Y codes and L2 Y codes are assumed to be down 3 and 6 dB, respectively) because of the squaring loss penalty of incomplete knowledge of the Y code. Even mild scintillation can cause loss of lock for typical S/N_0 encountered for low-elevation angle satellites. For the “strong” scintillation case ($\sigma_{\delta\phi} = 0.6$ rad) the loop barely maintains lock even at $S/N_0 = 44$ dB Hz.

Figure 12 shows the WAAS L1 C/A code RMS code tracking error (in meters) versus L1 C/A code signal-to-noise density ratio S/N_0 . Figure 13 shows the WAAS L1 carrier-tracking loop performance (the plotted results include 5.7° of oscillator-induced jitter). The main cause of the differences between the WAAS and GPS L1 figures is that the WAAS integration time is 2 ms while the GPS integration time is 20 ms.

5. Conclusions

This paper has presented scintillation signal and GPS-WAAS receiver models that were designed to

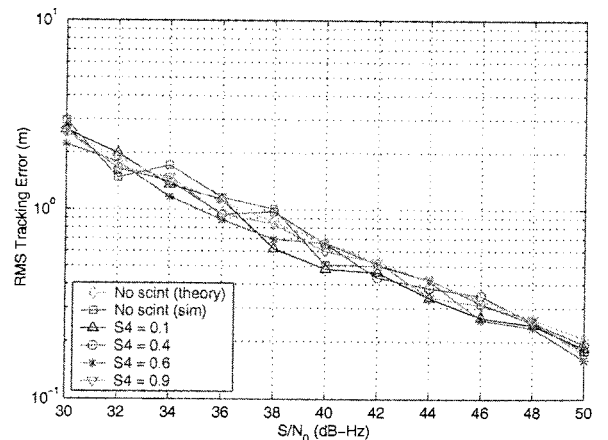


Figure 12. WAAS L1 C/A-code-tracking results.

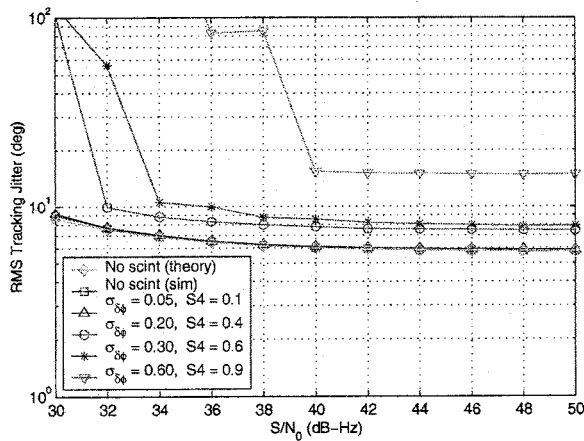


Figure 13. WAAS L1 carrier-tracking results.

provide insights into GPS-WAAS receiver performance degradations that occur in the presence of ionospheric scintillation. The scintillation signal model features direct generation of intensity and phase variation samples with desired marginal distributions and correlation properties. Spectral shaping is applied to achieve desired spectral properties. It was noted that the cross correlation of intensity variation and phase variation samples was reduced by the spectral shaping. Future work is being focused on the achievement of higher target cross-correlation levels, possibly through enhancement of the correlation of the samples prior to spectral shaping.

The results of receiver simulations indicate that the noncoherent DLLs typically employed by aviation-grade receivers are very robust to both amplitude and phase scintillation. Carrier-phase-tracking loops are much more susceptible to scintillation, and the signal-to-noise threshold for reliable carrier tracking is very dependent on the scintillation strength. Fortunately, it appears that the worst case scintillation typically encountered at midlatitudes, including the United States, will not significantly impact L1 carrier-tracking performance. Semi-codeless tracking of the L2 carrier has been shown to be very fragile. Even weak scintillation can cause loss of L2 carrier lock for low-elevation satellites. This effect is due to the need for L1 carrier aiding to overcome the signal-to-noise degradation inherent in tracking the L2 carrier without complete knowledge of the Y code. Scintillation can cause the L1 carrier phase and L2 carrier phase to lose coherence and invalidate the

assumption of common dynamics on L1 and L2 that allows the use of extremely narrow loop bandwidths for semicodeless L2 carrier tracking.

Acknowledgments. The authors would like to acknowledge the FAA GPS Product Team (AND-730), the sponsor of this work. This paper is based on system analysis studies performed for the FAA GPS Product Team (AND-730). This paper reflects the views of the authors. Neither the Federal Aviation Administration nor the Department of Transportation makes any warranty or guarantee, or promise, expressed or implied, concerning the content or accuracy of the views expressed herein. This work was produced for the U.S. Government under contract DTFA01-93-C-00001 and is subject to Federal Acquisition Regulation Clause 52.227-14, Rights in Data-General, Alt. III (JUN 1987) and Alt. IV (JUN 1987).

References

- Aarons, J., and S. Basu, Ionospheric amplitude and phase fluctuations at the GPS frequencies, in *Proceedings of ION GPS-94*, pp. 1569–1578, Inst. of Navig., Alexandria, Va., 1994.
- Basu, S., E. MacKenzie, S. Basu, E. Costa, P. Fougere, H. Carlson, and H. Whitney, 250 MHz/GHz scintillation parameters in the equatorial, polar, and auroral environments, *IEEE Selected Areas Commun., SAC-5(2)*, 102–115, 1987.
- Devroye, L., *Non-uniform Random Variate Generation*, pp. 405, 407–410, 416–418, and 588, Springer-Verlag, New York, 1986.
- Fremouw, E. J., R. C. Livingston, and D. A. Miller, On the statistics of scintillation signals, *Atmos. Terr. Phys.*, 42, 717–731, Pergamon, New York, 1980.
- Hatch, R., R. Keegan, and T. Stansell, Kinematic receiver technology from Magnavox, paper presented at 6th International Geodetic Symposium on Satellite Positioning, The Ohio State University, Columbus, Ohio, March 1992.
- Hegarty, C., Codeless GPS receiver performance investigation, *MITRE Memo. F061-M-299*, MITRE Corp., McLean, Va., November 14, 1994.
- Hegarty, C., Analytical Derivation of Maximum Tolerable In-Band Interference Levels for Aviation Applications of GNSS, *Navigation*, 44(1), 25–34, 1997.
- Holmes, J. K., *Coherent Spread Spectrum Communications*, Krieger, Melbourne, Fla., 1990.
- Kasdin, N. J., Discrete simulation of colored noise and stochastic processes and $1/f^\alpha$ power law noise generation, *Proc. IEEE*, 83(4), 802–827, 1995.
- Klobuchar, J., Ionospheric effects on GPS, in *Global Positioning System: Theory and Applications*, vol. 1, edited by B. Parkinson and J. Spilker Jr., pp. 485–515, Am. Inst. of Aeronaut. and Astronaut., New York, 1996.

- Loh, R., V. Wullschleger, B. Elrod, M. Lage, and F. Haas, The U.S. wide-area augmentation system (WAAS), *Navigation*, 42(3), 435–465, 1995.
- Nakagami, M., The m-distribution: A general formula of intensity distribution of rapid fading, in *Statistical Methods in Radio Wave Propagation*, edited by W. C. Hoffman, pp. 3–36, Pergamon, New York, 1960.
- Pullen, S., G. Opshaug, A. Hansen, T. Walter, P. Enge, and B. Parkinson, A preliminary study of the effect of ionospheric scintillation on WAAS user availability in equatorial regions, in *Proceedings of ION GPS-98*, Inst. of Navig., Alexandria, Va., 1998.
- Schmeiser, B. W., and R. Lal, Bivariate gamma random vectors, *Oper. Res.*, 30(2), 355–374, 1982.
- Secan, J. A., *WBMOD: Ionospheric Radiowave Scintillation Model, Version 13.04*, NorthWest Res. Assoc., Inc., Bellevue, Wash., 1996.
- Stephens, S. A., and J. C. Thomas, Controlled-root formulation for digital phase-locked loops, *IEEE Trans. Aerosp. and Electron. Syst.* 31(1), 78–95, 1995.
- Van Dierendonck, A. J., Understanding GPS receiver technology: A tutorial on what those words mean, paper presented at International Symposium on Kinematic Systems in Geodesy, Geomatics and Navigation, Univ. of Calgary, Banff, Alberta, Canada, Sept. 1994.
- Van Dierendonck, A. J., GPS receivers, in *Global Positioning System: Theory and Applications*, vol. 1, edited by B. Parkinson and J. J. Spilker Jr., pp. 329–407, Am. Inst. of Aeronaut. and Astronaut., New York, 1996.
- Van Dierendonck, A. J., P. Fenton, and T. Ford, Theory and performance of narrow correlator spacing in a GPS receiver, *Navigation*, 31(1), 265–283, 1992.
- Van Dierendonck, A. J., Q. Hua, P. Fenton, and J. Klobuchar, Commercial ionospheric scintillation monitoring receiver development and test results, in *Proceedings of the 52nd Annual Meeting*, pp. 573–582, Inst. of Navig., Alexandria, Va., 1996.
- Ward, P., Dual use of military anti-jam GPS receiver design techniques for commercial aviation RF interference integrity monitoring, *Navigation*, 41(4), 1995.
- Woo, K. T., Optimum semi-codeless carrier phase tracking of L2, *Navigation*, 47(2), 82–99, 2000.
-
- M. B. El-Arini, S. Ericson, C. Hegarty, and T. Kim, Center for Advanced Aviation System Development, The MITRE Corporation, 1820 Dolley Madison Boulevard, M/S W309, McLean, VA 22102-3481. (bakry@mitre.org; ericson@mitre.org; chegarty@mitre.org; tkim@mitre.org)

(Received December 21, 1999; revised February 13, 2001; accepted February 14, 2001.)

